

Massive High-Redshift Quiescent Galaxies With JWST

Themiyi Nanayakkara^{1*}, James Esdaile¹, Karl Glazebrook¹, Juan M. Espejo Salcedo¹, Mark Durre¹, Colin Jacobs¹

¹Centre for Astrophysics and Supercomputing, Swinburne University of Technology, Hawthorn, VIC 3122, Australia.

Abstract

Recent ground based deep observations of the Universe have discovered populations of massive quiescent galaxies at $z \sim 3 - 5$. The observed number density of sources are higher than predicted by cosmological models. Thus, constraining the formation and evolutionary mechanisms of these galaxies is crucial to determine how the Universe built such massive galaxies early in the Universe and what mechanisms drove the cessation of star-formation. With the scheduled launch of the *James Webb Space Telescope*, observations of rest-frame optical features of $z \sim 3 - 5$ galaxies will be enabled through the continuous $0.6 - 5.3\mu\text{m}$ coverage of the on-board NIRSpec instrument. Here we perform mock JWST/NIRSpec observations to determine optimal observing strategies to efficiently recover the completeness, star-formation histories, element abundances, and the initial mass function of massive quiescent galaxies in this cosmic window. We show that through smart grism/filter choices, NIRSpec slit and integral field spectroscopy observations can be used to constrain formation pathways of these galaxies to high accuracy with high efficiency. Such observations could revolutionize our understanding of galaxy evolution in the early Universe providing much needed constraints to galaxy evolutionary models in the early Universe.

Keywords: Infrared observatories – High-redshift galaxies – Quenched galaxies – Galaxy evolution – Chemical abundances

1 INTRODUCTION

The development of sensitive near-infrared imaging instruments such as Magellan/FourStar (Persson et al., 2013), VLT/HAWK-I (Kissler-Patig et al., 2008), ESO/VISTA (Sutherland et al., 2015) and UKIRT/WFCAM (Casali et al., 2007) opened a new window into the Universe with detections of the first populations of red galaxies at $z \sim 3 - 5$ (e.g. Marchesini et al., 2010; Spitler et al., 2014; Straatman et al., 2014; Patel et al., 2017). The first photometric confirmations from these surveys suggested a high abundance of massive quiescent galaxies in the early Universe posing a challenge to current cosmological simulations (Sparre et al., 2015; Wellons et al., 2015; Davé et al., 2016; Merlin et al., 2019). These tensions arise due to the short star-formation time scales of these galaxies, which would require them to have formed the bulk of their stars with stellar masses up to $\sim 10^{11}M_{\odot}$ and have undergone subsequent cessation of star-formation within the first two billion years of the Universe. Galaxy evolution and mass buildup within such a short time-frame has strong implications for cosmological and chemical evolutionary models of the Universe, making massive $z \sim 3 - 5$ quiescent galaxies ideal laboratories to determine how galaxies grew and what mechanisms shut down star-formation in the early Universe.

Given the many challenges the abundance of $z \sim 3 - 5$ quiescent galaxies pose to current cosmological frameworks of the Universe, obtaining spectroscopic confirmations of their abundance is vital. In addition, a detailed understanding of the stellar population properties of the $z \sim 3 - 5$ massive quiescent galaxies and their formation mechanisms can only be obtained through spectroscopy. Glazebrook et al. (2017) used deep Keck/MOSFIRE observations to spectroscopically confirm the very first massive quiescent galaxy in the $z > 3$ Universe. Their results showed that this galaxy was likely formed in a major star-formation event at $z > 5$, with a star formation rate (SFR) exceeding $1000M_{\odot}/\text{yr}$, posing a significant challenge to models. Subsequent studies have now started to build up samples of spectroscopically confirmed massive quiescent galaxies at $z \sim 3 - 4$ (e.g. Marsan et al., 2017; Schreiber et al., 2018; Tanaka et al., 2019; Forrest et al., 2020a,b; Valentino et al., 2020).

Spectroscopic confirmations of several massive $z \sim 3 - 5$ quiescent galaxies have further strengthened the need for galaxy formation models to provide efficient mass buildup and subsequent quick quenching mechanisms (e.g Davé et al., 2016; Merlin et al., 2019). Formation timescales for these galaxies is an important quantity to be constrained as extended formation allows the galaxy to be assembled gradually in a hierarchy of mergers relieving the tension with

*E-mail: themiyananayakkara@gmail.com

current models. Star formation history (SFH) analysis suggest average formation timescales of $\lesssim 200$ Myr, which poses a challenge to early galaxy formation models (Glazebrook et al., 2017) and hierarchical models cannot produce these massive galaxies in a single rapid event.

Rest-frame optical spectra are the gold standard required to reconstruct the formation history of quiescent galaxies. This wavelength regime covers a variety of important absorption features which can be compared with stellar evolutionary models to determine the star-formation time scales and elemental abundances (Conroy, 2013). Balmer absorption lines have a strong dependence on the age and the SFH of galaxies (Poggianti & Barbaro, 1997). The variety of metal absorption lines such as Mg, Na, Ca, Ti, Na, and Fe observed in the rest-frame optical can be linked to properties of previous star-formation episodes using chemical evolution models (de La Rosa et al., 2011; Segers et al., 2016). Additionally, some of these features are sensitive to different types of stars, thus they can be used to infer stellar abundances and hence the initial mass function (IMF) of these galaxies (e.g. La Barbera et al., 2013).

If these massive $z \sim 3 - 5$ quiescent galaxies were built up in a short star-formation episode, it is likely that they were built from the early pristine gas of the Universe. Given the extreme low-metallicity gas and high SFRs in the early Universe, formation of massive stars would have been preferred (e.g. Narayanan & Davé, 2012). Therefore, it is plausible that chemical signatures in these galaxies would point towards enrichment through core-collapse supernovae (Nomoto et al., 2006) leading to an enhancement of α -elements in the interstellar medium (ISM) and stars (e.g. Kriek et al., 2016). Core collapse supernovae are end of the life products of short lived ($\sim 10 - 50$ Myr) massive stars and produce α -elements through supernovae nucleosynthesis. Longer lived (> 0.1 Gyr) lower mass stars result in Type-Ia supernova and produce heavier elements such as Fe through supernova nucleosynthesis (Kobayashi & Nomoto, 2009). Therefore, when the star-formation episodes are shorter than ~ 1 Gyr, the new stars formed from the gas in the enriched ISM would be α -enhanced and would lack of Fe. Thus, if spectral signatures of massive $z \sim 3 - 5$ quiescent galaxies show distinct enhancement in α -elements, this would suggest that these galaxies were likely formed in a short star-formation episode even if the IMF is unchanged.

The abundance of massive quiescent galaxies at $z \sim 3 - 5$ also has strong implications to the reionization and chemical evolutionary history of the Universe. If these galaxies are α -enhanced, this suggest that the latter generations of stars that built up the bulk of the $\sim 10^{11} M_{\odot}$ mass are likely to be from more massive stars with less Fe blanketing and less stellar winds in the atmospheres (Steidel et al., 2016). Therefore, these stars would have produced higher amounts of ionizing photons compared to solar α -abundance stars (Pauldrach et al., 2001). Additionally, core collapse supernovae has higher IMF averaged ejecta mass compared to Type Ia supernovae, which leads to stronger feedback mechanisms in galaxies

(Hopkins et al., 2018). This leads to creating more possibilities within the geometry of galaxies to create holes for ionizing photons to escape. The enhancement of ionizing photons along with strong supernova feedback driven changes in the ISM geometry may alter the contribution of massive galaxies to the reionization of the Universe at $z > 6$ (Naidu et al., 2019). Thus, if the high abundance of $z \sim 3 - 5$ massive quiescent galaxies is spectroscopically confirmed, the time-scales for the reionization of the Universe could alter leading to newer challenges in cosmology.

Kinematical properties of $z \sim 3 - 5$ massive quiescent galaxies also provide clues to the formation history of these early galaxies. Deep rest-frame optical spectra have opened the door to obtaining velocity dispersion measurements of massive quiescent galaxies at $z > 3$ (Tanaka et al., 2019; Esdaile et al., 2020; Saracco et al., 2020). When the $z > 3$ quiescent galaxies are compared in the size-mass plane, they require a greater size evolution compared to what is expected from minor mergers and shows evidence for dynamical masses to be lower than the stellar mass estimates (Esdaile et al., 2020). Additionally, despite sharing similar attributes as local elliptical galaxies, namely red colours and high stellar masses, there are indications that the morphology of high-redshift massive quiescent galaxies are quite different. Using the modeled axis-ratio from *HST* imaging shows indications of flattened ‘disc-like’ morphology in massive quiescent galaxies at $z > 3$ (Hill et al., 2019). If these galaxies are formed in short durations, mass growth through mergers would be uncommon, thus, disc-like morphologies would be prominent at high redshift. However, morphological constraints at $z > 3$ are poor because existing high resolution size measurements are based on rest-frame UV and susceptible to under estimation from potential dust-reddening or over estimation from recent star-formation events. Rest-frame optical size measurements, which trace older stellar mass, provide more robust measurements of size (Kubo et al., 2018). However, none of the current observations probe galaxies at sufficient depth and/or at the appropriate rest-frame wavelength windows to access features that could provide stronger constraints to the formation timescales (e.g. Schreiber et al., 2018; Forrest et al., 2020a; Carnall et al., 2020) or morphologies.

The launch of the *James Webb Space Telescope (JWST)* in 2021 provides a unique opportunity to explore the rest-frame optical spectral range of $z \sim 3 - 5$ massive quiescent galaxies. The continuous spectral coverage of NIRSpec from $0.6 - 5.3 \mu\text{m}$ (Birkmann et al., 2011) combined with its multiplexing capabilities, high sensitivity, and low thermal background, along with the lack of atmospheric contamination in space enables JWST to obtain high quality near-infra-red (NIR) spectroscopy of galaxies in the early Universe with high efficiency. Thus, by obtaining spectroscopic confirmations for photometrically selected candidates, JWST will enable astronomers to provide tighter constraints to the formation histories, stellar populations, and kinematics of $z \sim 3 - 5$ quiescent galaxies.

In this paper we explore how JWST could enable advances

in the $z \sim 3 - 5$ massive quiescent galaxy field based on samples confirmed by Schreiber et al. (2018). In Section 2 we discuss how JWST could be optimally used to confirm the redshift and quiescence of the photometrically selected quiescent galaxies. In Section 3 we discuss how JWST could enable detailed analysis of element abundances, star-formation histories, and the stellar initial mass functions (IMFs) of these galaxies and present optimal observing strategies. In Section 4 we discuss how JWST slit and integral field unit (IFU) spectroscopy could constrain the dynamics of these galaxies and in Section 5 we briefly discuss the expected advancements in the field with JWST and provide our conclusions. We assume a cosmology with $H_0 = 70 \text{ km s}^{-1} \text{ Mpc}^{-1}$, $\Omega_\Lambda = 0.7$, and $\Omega_M = 0.3$. We use AB magnitudes throughout the paper.

2 PROBING THE COMPLETENESS WITH JWST

2.1 The need for spectroscopic confirmations

Deep multi wavelength surveys utilizing medium-bands (such as ZFOURGE (Straatman et al., 2016)) have demonstrated that with photometric data, redshifts and evolutionary types of galaxies (i.e. blue/red star-forming or quiescent) can be inferred with high-accuracy (e.g. Spitler et al., 2014; Straatman et al., 2014). However, to constrain the number density of massive quiescent galaxies in the $z \sim 3 - 5$ epoch and rule out outliers, more precise redshift determinations along with quiescent indications are necessary (e.g. Schreiber et al., 2018). Therefore, obtaining spectroscopic confirmations and indications for quiescence in the spectra are crucial to make robust comparisons with cosmological models.

The main limitation of purely characterizing quiescent galaxies based on photometry is the redshift uncertainty. In SED fitting techniques, the shape of the multi-wavelength photometry is used to infer the redshift. Prominent breaks such as the Lyman and Balmer breaks and the D4000 features have shown to constrain the redshift at $\sim 2\%$ accuracy (e.g. Straatman et al., 2016). However, degeneracies between redshift and galaxy type adds uncertainty to the photometric redshift determination process. For example, as shown by Figure 1, the SED shape of $z \sim 2$ dusty (red) star-forming galaxies (e.g. Spitler et al., 2014) is largely similar to that of quiescent galaxies at $z \sim 4$. The Balmer break of $z \sim 4$ galaxies observed in the K -band could provide some constraints, however, the uncertainties in constraining the redshift and strong $H\alpha$ emission that contaminate $z \sim 2$ K -band photometry limits the diagnostic power. These outliers can be identified through emission lines which can be obtained with relatively short integration times. Thus, through spectroscopy these outliers can be identified and the evolution of number density of massive quiescent galaxies with cosmic time can be constrained.

In addition to the spectroscopic confirmation of the redshift, spectroscopy provides crucial coverage of important spectral features that determines the quiescence of galaxies. In Figure 2, we show the wavelength coverage of spectral features that

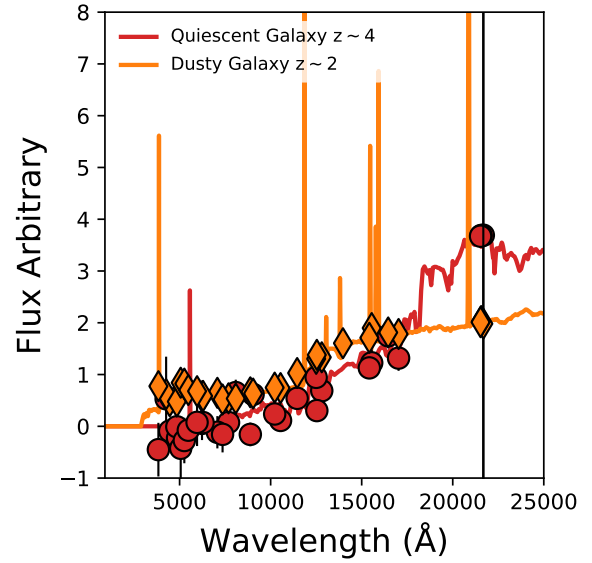


Figure 1. Two example SEDs from the ZFOURGE survey. Shown in red is a quiescent galaxy SED at $z \sim 4$ and in orange is a dusty star-forming galaxy at $z \sim 2$. Purely based on photometry, the normalized SEDs of the $z \sim 4$ quiescent and $z \sim 2$ dusty star-forming at $\lesssim 2\mu\text{m}$ looks largely similar, thus distinguishing between the two requires spectroscopy.

are necessary to determine the quiescence and the stellar population properties of $z \sim 3 - 5$ quiescent galaxies. By obtaining coverage of Balmer lines or forbidden lines such as $[\text{O III}]$ and $[\text{O III}]$, strong constraints can be placed on the levels of star-formation in these massive quiescent candidates. Absorption features of α -elements and other metals provide information on the stellar populations which is crucial to determine the star-formation history of these galaxies. With redshift and star-formation constrained through spectroscopy, multi-wavelength SED fitting would provide stronger constraints to stellar masses and SFHs of these galaxies, which are also important parameters to test the cosmological evolution models.

2.2 NIRSpec CLEAR spectroscopy as a redshift confirmation machine

In order to address the number density of massive quiescent galaxies in the $z \sim 3 - 5$ epoch, a systematic spectroscopic follow up of all massive quiescent galaxy candidates is required. Rest-frame $U - V$ vs $V - J$ colour distributions have shown to be effective in identifying the star-forming and quiescent galaxies from each other in various cosmic epochs (e.g. Williams et al., 2009; Straatman et al., 2014). Recent ground based efforts have been successful in obtaining the rest-frame optical coverage of the brightest of these quiescent candidates (e.g. Schreiber et al., 2018; Valentino et al., 2020) and have shown high success rate in identifying quiescent galaxies based on rest-frame UVJ colours with a high purity but not necessarily high completeness. For example Schreiber

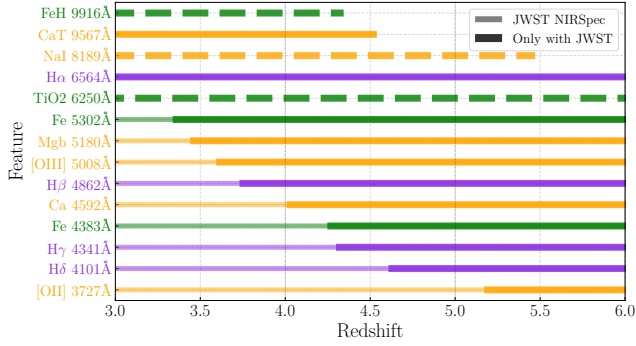


Figure 2. JWST NIRSpec wavelength coverage of rest-frame optical features that are crucial to determine the quiescence and to constrain the stellar population properties of massive $z \sim 3 - 5$ quiescent galaxies. Redshifts only accessible via space-based spectroscopy of JWST are shown by the thicker/darker color lines. Balmer emission/absorption features (sensitive to the SFH) are labeled in purple, forbidden emission lines and α -element absorption lines are labeled in orange, while the other absorption features that constrain the overall stellar metallicity are labeled in green. It is evident that JWST NIRSpec spectroscopy is crucial to obtain a suite of spectral features that are necessary to analyze the $z \sim 3 - 5$ quiescent galaxy populations.

et al. (2018) analyzed 24 UVJ selected galaxies and obtained redshift confirmations 12 galaxies out of which only two were $z \sim 2$ dusty star-forming interlopers (see discussion in Schreiber et al. (2018)).

However, studies have so far only targeted the brightest quiescent galaxies in the $z \sim 3 - 5$ epoch. This is driven by observational challenges in obtaining ground based NIR spectroscopy. The limited wavelength coverage due to atmospheric absorption, strong sky line contamination, along with limited multiplexing capabilities in ground based NIR instruments have traditionally challenged astronomers to spectroscopically follow up mass/magnitude complete samples of quiescent galaxies. Additionally, targeting only the brightest galaxies biases the samples since the most massive galaxies are in general older and fainter at a given mass.

The multiplexing capability and the continuous $0.6 - 5.3 \mu\text{m}$ coverage makes JWST/NIRSpec an ideal instrument to obtain spectroscopic redshifts of photometrically selected massive quiescent galaxy candidates. By selecting quiescent candidates from deep ground and space-based imaging surveys, NIRSpec CLEAR spectroscopy can obtain the crucial rest-frame optical absorption features that are necessary to confirm the redshifts, quiescence, and rule out low-redshift interlopers. In the case of interlopers, as discussed in Section 2.1, the primary contaminants are dusty star-forming galaxies at $z \sim 2$, which will show $H\alpha$ and other strong emission lines in short exposure times.

In Figure 3 we show that NIRSpec CLEAR spectroscopy is capable of accurately distinguishing between quiescent, post-starburst, and star-forming SEDs and measuring spectral features to confirm the quiescence. Strong Balmer and forbidden emission features prominent in star-forming galaxies will be detectable by $R \sim 100$ spectroscopy to rule out any star-forming contaminants. $H\beta$ and $H\gamma$ absorption features can be used to determine the time since the last star-formation

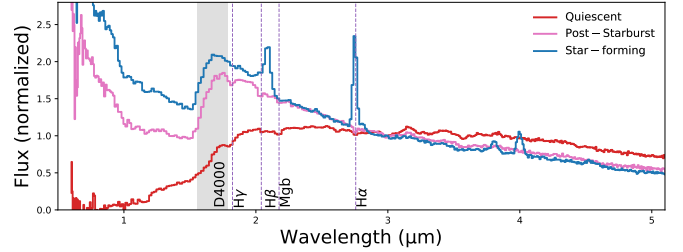


Figure 3. Simulated observations of NIRSpec CLEAR spectroscopy for a quiescent, a post star-burst, and a dusty star-forming galaxy at $z \sim 3$. All these galaxies may have redder NIR colours due to age-dust degeneracies, thus distinguishing between them purely based on photometry is challenging. The high sensitivity coupled with the multiplexing capability makes NIRSpec and ideal instrument to obtain $0.6 \mu\text{m} - 5.3 \mu\text{m}$ spectroscopy to accurately distinguish between these types of galaxies and confirm the quiescence. The spectra shown here are all normalized to $K = 21.5$ and the typical continuum S/N obtained with NIRSpec CLEAR spectroscopy is $\sim 80 - 100$ in a ~ 1500 s exposure.

episode (e.g. Glazebrook et al., 2017) and comparisons of the continuum around D4000 feature and the rest-frame near-UV continuum can distinguish between post-starburst and star-forming galaxies.

In addition to the simultaneous $0.6 - 5.3 \mu\text{m}$ wavelength coverage, the sensitivity of the NIRSpec instrument and the lower background level in space-based observations increases the efficiency of the JWST observations. Spectra shown in Figure 3 are normalized to $K = 21.5$ and in ~ 1500 s NIRSpec CLEAR spectroscopy, a typical continuum S/N of $\sim 80 - 100$ can be achieved. Glazebrook et al. (2017) obtained a S/N of 6 for a $K = 22.5$ $z = 3.7$ quiescent galaxy with 7 hours of K -band Keck/MOSFIRE spectroscopy at a resolution of 19\AA per pixel. For a $K = 21.5$ source Keck/MOSFIRE can reach a S/N of ~ 9 in 1500s at similar resolution to NIRSpec CLEAR spectroscopy. Therefore, even when only a limited wavelength coverage is considered, NIRSpec CLEAR spectroscopy is $\sim \times 10$ more efficient.

As a potential caveat to the efficiency of quiescent galaxy surveys using NIRSpec CLEAR, we also note that the NIRSpec MSA adds extra observational challenges in obtaining uncontaminated spectra of galaxies. In addition to contamination from fixed open shutters, as stated in JDox MSA flux leakage due to small gaps in the MSA shutters can lead to $\sim 2\%$ contamination¹. Therefore, to obtain deep spectroscopy of faint spectral features, the NIRSpec Fixed Slits (S200A1 or S200A2 with $0.2''$ slit width) is ideally suited. Fixed Slits provide the cleanest spectra in the NIRSpec detectors and yields a higher S/N compared to the MSA mode for the same exposure time. Additionally, it is possible to obtain simultaneous MSA and fixed slit spectroscopy by positioning the primary target of interest in the fixed slit location and populating the MSA shutters with secondary targets by either configuring the MSA by only allowing rotational variation in the MSA Planning

¹https://jwst-docs.stsci.edu/near-infrared-spectrograph/nirspec-instrumentation/nirspec-micro-shutter-assembly#NIRSpecMicro-ShutterAssembly-msa_leakageMSAfluxleakage

design tool or by manually configuring the MSA shutters in open/close positions.

3 STELLAR POPULATIONS WITH JWST

Stellar population properties of galaxies can be obtained via rest-UV and optical absorption line spectroscopy. Due to the short lifetimes of O and B type stars which contribute to UV flux, rest-frame optical features from A and G type stars play the most important role in deciphering the underlying stellar population properties of quiescent galaxies. In Figure 4, we show prominent rest-frame optical absorption lines that are necessary to constrain the ages, metallicities, and element abundances of quiescent galaxies. These model spectra are computed from Villaume et al. (2017) empirical SSPs using the `alf` software (Conroy et al., 2018). It is clear from the figure that not all features differ substantially between models such that they can be distinguished at a given sensitivity. As an example, the SFH (or rather the time since the last star formation episode) can be well constrained by the Balmer absorption lines with reasonable S/N limits (~ 100). However, in order to map changes in the lower-mass IMF slope through the IMF sensitive features such as the Fe-H band and NaD absorption (e.g. Conroy & van Dokkum, 2012) requires extremely high S/N sensitivity of $\gtrsim 350$. Achieving such levels of S/N in spectroscopy for populations of galaxies at $z > 3$, even with JWST requires upwards of hundreds of hours per target and is not practical.

In the following Section 3.1 we go beyond individual spectral line analysis and perform full spectrum fits to identify optimal S/N levels and JWST/NIRSpec grism/filter combinations required to constrain the element abundances and the SFH of $z \gtrsim 3$ quiescent galaxies. The combined role of spectroscopy and multi-wavelength photometry in constraining the complex SFH of galaxies will be addressed in Section 3.2.

3.1 Element abundances

Rest-frame optical spectroscopy covers the spectral features that are necessary to constrain the formation history of quiescent galaxies. In addition to constraining the last star-formation episode from the Balmer absorption features, the coverage of absorption features from elements such as Mg, Fe, Ti provides additional constraints to the durations of previous star-formation episodes, metallicities and chemical abundance patterns of galaxies (e.g. Vazdekis et al., 2010). These are crucial to determine whether these early massive quiescent galaxies were formed in single star-formation episodes, or whether they were formed in extended SFH episodes. The latter would help relieve the tension with Λ CDM hierarchical galaxy formation models.

To determine optimal JWST NIRSpec grism/filter combinations and S/N thresholds required to accurately obtain element abundances, we use Villaume et al. (2017) empirical SSPs to generate a mock 1.5 Gyr old galaxy at $z = 3.2$. We add a velocity dispersion of 300 km/s to the galaxy and

keep all elemental abundances at solar. We feed the mock galaxy to the JWST exposure time calculator (ETC) to obtain a suite of mock observables at different S/N values for the JWST NIRSpec fixed slit S200A1 with G235H/FL170LP and G395H/FL290LP grism/filter combinations. We then use the full spectral fitting code `alf` (Conroy et al., 2018) on the calibrated data to fit for velocity, velocity dispersion, age, $[Z/H]$, and the abundances of the elements C, N, O, Mg, Si, Ca, Ti, and Na. Spectral fitting is performed to each individual grism/filter combination and to the combined spectrum.

In Figure 5 we show the element abundance recovery of $[Mg/Fe]$, $[Ti/Fe]$, and $[Fe/H]$ for our mock observables. It is evident that at native resolutions of each grism/filter combination with $S/N \gtrsim 30$ per pixel, the recovery of the elemental abundances converge to the input values. We further find that there is no significant difference between the two grism/filter combinations. However, when the spectra from both grism/filter combinations are fit together, the uncertainty is slightly decreased. Even though spectral features such as Mgb are not covered by G395H/FL290LP for $z = 3.2$ galaxies, inherent relationships between various α -elements and other metals in the Villaume et al. (2017) templates allows Mg abundance to be converged albeit with slight systemic offset. For example because Mg and Ca are both α elements, the coverage of the CaT λ 8498.18542.18662 features can be used to constrain the Mg abundance using theoretical response functions (Conroy et al., 2018). Thus, abundances of elements not included in the spectral range are inferred from predetermined element abundance ratios and chemical evolutionary models. However, direct measurements of element abundances should be preferred particularly for high redshift galaxies where these assumptions may not hold.

We conclude that, at $z \sim 3 - 5$ most spectral features that are necessary to obtain α -element abundances can be obtained by the G235H/FL170LP grism/filter combination. Next, we investigate whether the choice of spectral resolution determined by the G235M and G235H grisms play a significant role in the convergence of mock observable parameters. In Figure 6 we show the recovery of the parameters for the G235M and G235H grisms. It is evident that there is no significant difference between the two grisms for the recovery of the $[Mg/Fe]$, $[Ti/Fe]$, and $[Fe/H]$ element abundances. Thus, it is advantageous to obtain G235M spectroscopy to increase the efficiency of $z > 3$ quiescent galaxy observing programs. From our ALF simulations we find that at a S/N of ~ 30 per pixel an accuracy of $\sim 15\%$ can be obtained for element abundances which is comparable to the accuracy obtained for local globular clusters (Conroy et al., 2018).

In Figure 7 we show the simulated JWST/NIRSpec G235M/FL170LP observations of the four $z \sim 3 - 4$ quiescent galaxies from the Esdaile et al. (2020) sample. These galaxies have per pixel $S/N \sim 5 - 10$ in ground based spectra with exposure times up to ~ 15 h with Keck/MOSFIRE. Following morphological properties derived by Esdaile et al. (2020), we reconstruct each source on the JWST ETC based on the

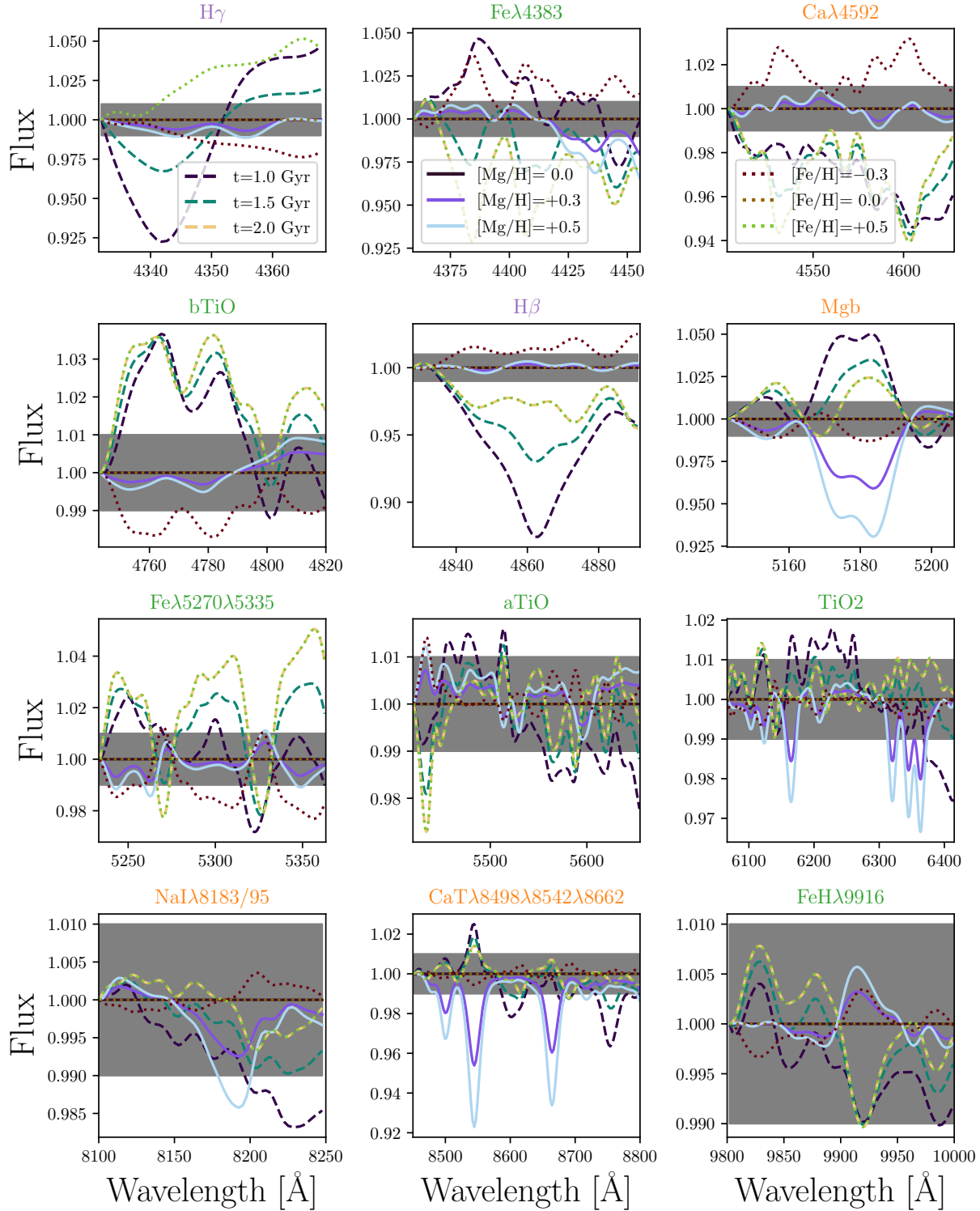


Figure 4. Here we show Villaume et al. (2017) empirical SSPs computed at different ages (dashed), α -abundances (solid), and metallicities (dotted) using ALF. Spectra and smoothed to a resolution of 100 km/s and are divided by a 1.5Gyr old solar abundance spectrum, so relative changes in the spectra can be clearly identified. The grey shaded region shows the relative accuracy that is obtained by a S/N=100 spectrum. It is evident that age through the Balmer absorption lines, α -abundances through Mgb, and metallicity ($[Fe/H]$) through Fe features can be recovered using through these individual absorption features at this S/N level.

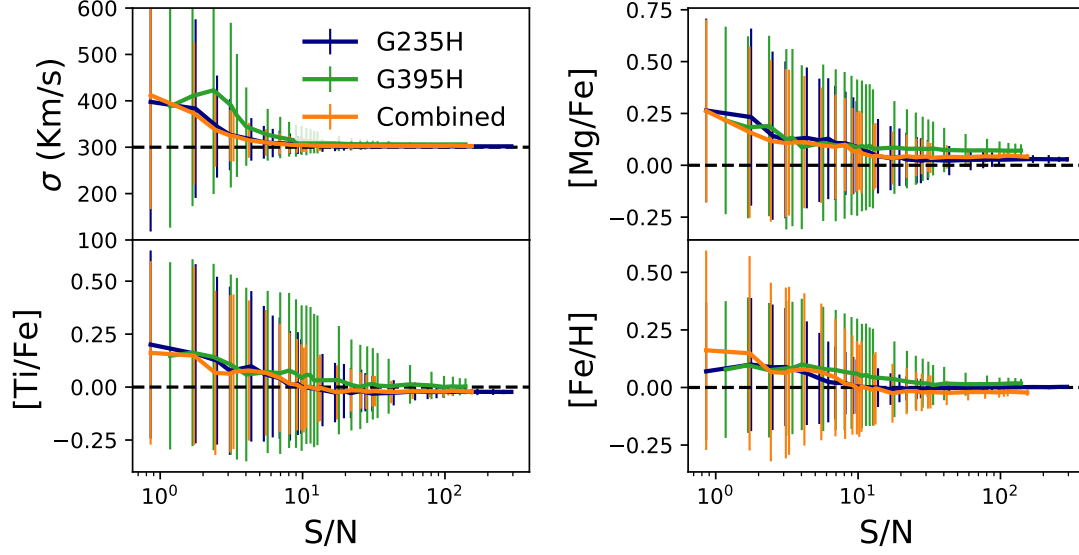


Figure 5. The recovery of **Top Left:** velocity dispersion and elemental abundances of **Top Right:** [Mg/Fe], **Lower Left:** [Ti/Fe], **Lower Right:** [Fe/H] of mock JWST NIRSpec S200A1 G235H/FL170LP and G395H/FL290LP observations. Full spectral fitting is performed using `a1f` Conroy et al. (2018) for individual grism/filter combinations separately and together at their respective grism native resolutions. The input values to the model spectra are shown by the horizontal dashed lines.

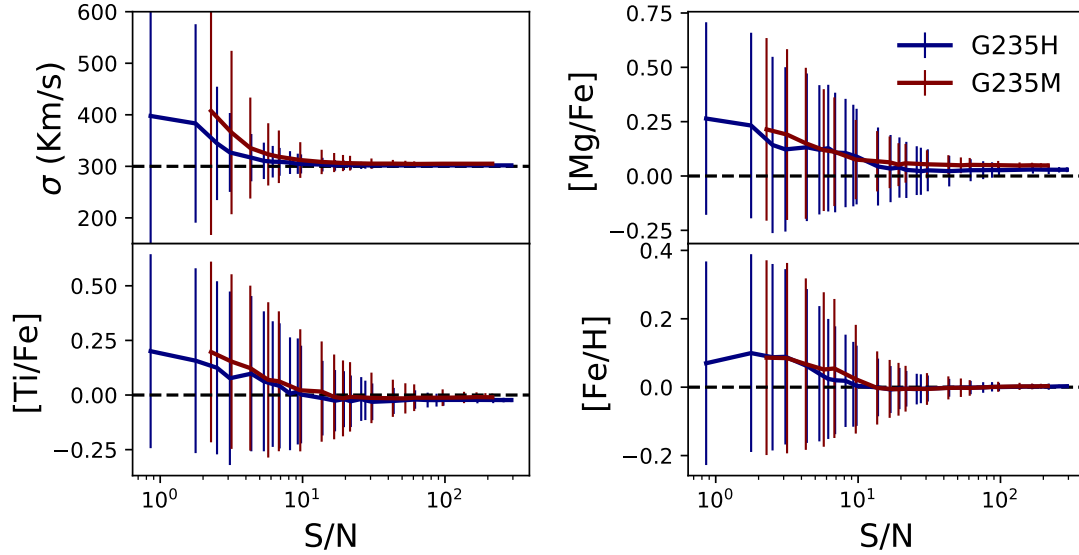


Figure 6. The recovery of **Top Left:** velocity dispersion and elemental abundances of **Top Right:** [Mg/Fe], **Lower Left:** [Ti/Fe], **Lower Right:** [Fe/H] from NIRSpec G235M/FL170LP and G235H/FL170LP grism/filter combinations using `a1f` (Conroy et al., 2018) at their respective grism native resolutions. The true value is shown by the horizontal dashed lines. It is evident that the even with the lower resolution G235M grism, the input parameters can be accurately recovered at $S/N \gtrsim 30$. Given the S/N can increase by a factor of $\gtrsim 2$ between G235H and G235M, obtaining absorption line spectroscopy of massive quiescent galaxies using the G235M will be the most efficient without compromising the scientific goals.

HST WFC3/F160W imaging and use the best fit FAST++² spectra from Schreiber et al. (2018) as the source spectra. Following our aforementioned experiments with `alf`, we alter the exposure times to obtain a continuum S/N ~ 30 – 40 , which is the required S/N to obtain accurate recoveries of spectral parameters. With exposure times ranging between 4 – 8 h, JWST/NIRSpec G235M/F170LP provide $\gtrsim 7$ times better S/N at similar velocity resolutions compared to ground based Keck/MOSFIRE spectra. It is also clear from the figure that, space-based observations from JWST allows a continuous coverage of most crucial rest-frame optical spectral signatures for the $z \sim 3$ – 4 quiescent galaxy populations. These range from age, α -element abundance, and overall metallicity sensitive indicators and are shown in Figure 4. Thus, with modest JWST observations, rest-frame optical spectra of $z > 3$ quiescent galaxies can be obtained to constrain their formation and evolution properties with high confidence.

3.2 SFH

There is significant tension regarding the existence and abundance of massive quiescent galaxies in the $z > 3$ universe between observations and cosmological simulation models (e.g. Merlin et al., 2019). Thus, determining how these massive quiescent galaxies built their mass efficiently is of the highest priority if we seek to understand the formation and subsequent quenching mechanisms of these galaxies.

The star formation history of massive quiescent galaxies at $z \sim 3$ – 5 could be addressed via two different methods. Firstly, through analysis of individual line strengths such as Balmer, D4000 features allows approximate durations of the most recent SFH to be constrained (Vazdekis et al., 2015). Additionally, if an enhancement of α -elements such as Mg, Ca, and Na is observed, this would provide indications that they were formed over a short starburst event due to the delay time of Type Ia supernovae (e.g. Kriek et al., 2016).

Secondly, more stringent constraints to the SFHs can be made by combining full spectrum fitting techniques with multi-wavelength photometric fitting techniques. However, even full spectrophotometric fitting techniques have degeneracies which results in factor of a ~ 2 uncertainty in derived cosmological parameters such as the cosmic star formation rate density (e.g. Madau & Dickinson, 2014; Yu & Wang, 2016). This is a result of multiple levels of complex degeneracies and uncertainties inherent to stellar populations models (Conroy, 2013) and SED fitting techniques (Walcher et al., 2011). If only photometry is used in SED fitting, inferences are based on purely the SED shape. This can result in systematic offsets in derived galaxy properties due to effects such as the age-dust-metallicity degeneracy that affects the shape of the SED (Bell & de Jong, 2001).

When spectra are combined with the photometry, stronger inferences can be made on galaxy properties due to extra information that can be obtained from the spectral features.

However, uncertainties in stellar evolution, limitations in empirical stellar libraries, and limitations in theoretical stellar atmosphere models can introduce systematic biases to the inferences (e.g. Bruzual, 2007). The SFH of a galaxy will have imprints in the overall shape of the SED and on the strength of element abundances of the spectra. Additionally, the presence of specific types of stars leaves wider spectral imprints which can be used to provide further constraints (e.g. Brinchmann et al., 2008). However, simultaneous modeling of a variety of spectral features that consider variations in stellar types, stellar/ISM abundances, and IMFs is complicated (Gunawardhana et al., 2020) and when combined with non-parametric SFHs to model the formation history, high quality data and modular SED fitting codes become crucial (e.g. Leja et al., 2017).

To investigate whether spectrophotometric fitting could recover the SFHs to accurately distinguish between hierarchical merger formation vs single burst formation, we use the FSPS code (Conroy & Gunn, 2010) to generate synthetic spectra to create mock observables. We note that FSPS does not allow individual element abundances to be varied. The first galaxy is formed through a complex SFH with constant and exponentially declining SFH components and undergoes a burst in the final Gyr. This mimics a post-starburst galaxy formed through hierarchical assembly. The second galaxy is formed via a single burst event at $t=0$ and would challenge Λ CDM cosmology. Both galaxies are observed at an age of 1.5 Gyr. The mock NIRSpec observations are made using the JWST ETC with the exposure time tuned to obtain a S/N ~ 30 per pixel and the output spectra are instrument throughput corrected and flux calibrated.

Utilizing the deep NIRSpec rest-frame optical spectra with full spectrum fitting techniques of PROSPECTOR (Johnson et al., 2020) and its non-parametric approach to constraining the star formation histories (e.g. Leja et al., 2019), we investigate whether precise constraints could be placed on the formation timescale of massive quiescent galaxies. Corresponding multi-wavelength photometry for the galaxies are computed using `sedpy` python package mirroring the full wavelength coverage of the ZFOURGE COSMOS field (Straatman et al., 2016). All photometric bands are expected to be detected at a S/N of 10. PROSPECTOR fitting is performed using a non-parametric SFH with 15 free parameters which includes 6 SFH bins. In Figure 8 we show the MCMC corner plots for the two galaxies. The posterior of both galaxies are sampled well and shows no strong degeneracies between the parameters. We additionally perform PROSPECTOR fitting utilizing only 3 SFH bins and their MCMC corner plots are shown by Figure 9.

In Figure 10 we show the recovery of the SFH for the two galaxies. For the single burst galaxy, recovered SFH with 6 SFH bins matches well with the input SFH. However, when the galaxy spectra and photometry are fit with 3 SFH bins, the recovered SFH deviates significantly from the input SFH. This is opposite to what is observed for the galaxy with a composite SFH, where the SFH recovered from the 6 SFH bins shows

²<https://github.com/cschreib/fastpp>

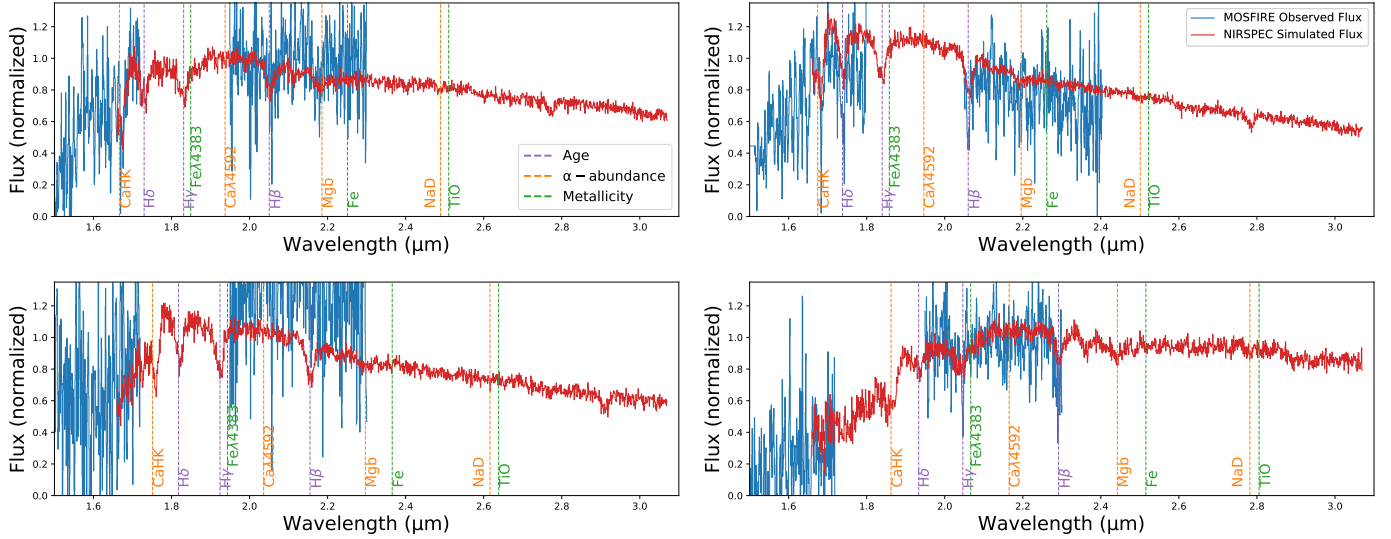


Figure 7. Simulated JWST NIRSpec G235M/FL170LP observations of the four $z \sim 3 - 4$ quiescent galaxies presented by Esdaile et al. (2020). The best fit FAST++ templates to the galaxies from Schreiber et al. (2018) are used to obtain the JWST mock observations. We show **Top Left:** 3D-EGS-40032 ($\sim 8h$), **Top Right:** 3D-EGS-18996 ($\sim 4h$), **Lower Left:** 3D-EGS-31322 ($\sim 4h$), and **Lower Right:** ZF-COSMOS-20115 ($\sim 5h$) where the time stated inside the brackets refer to the typical NIRSpec G235M/FL170LP observing times necessary to obtain a continuum S/N of $\sim 30 - 40$. Ground based H and K band Keck/MOSFIRE spectra from Schreiber et al. (2018) are also shown for comparison. With < 10 h JWST/NIRSpec can obtain ≥ 7 times greater S/N quality at similar velocity resolutions compared to the current ground-based data for such targets and provides a continuous coverage of features through atmospheric windows which are essential to analyze the stellar population properties of these galaxies. These features are colour coded according to their primary sensitivity to age, α -abundance, and metallicity.

an increase in SFH in the final ~ 700 Myr. The input SFH is recovered well with 3 SFH bins. These differences are likely due to the sensitivity of certain photometric/spectral features to the SFH which are enhanced with finer/coarse time sampling.

We conclude that in order to recover the input SFHs accurately, some tuning of the number of SFH bins are required. However, these should be well tested with simulated models for galaxies with short evolutionary times (age $\lesssim 3$ Gyr) and we defer this to a future analysis. We note that the rest-frame optical includes both age and abundance-sensitive lines, thus both the SFH and metallicity can be constrained to high accuracy using PROSPECTOR with fine tuned binning. Additionally, when direct α -element constraints are lacking, metallicity along with strong constraints on the SFH can be used to infer the α -abundances.

3.3 The IMF

The stellar initial mass function is a fundamental parameter in galaxy evolution that plays a vital role in regulating galaxy formation and chemical evolution of the Universe. Even though traditionally the IMF has been considered to be Universal (e.g. Salpeter, 1955; Kroupa, 2001; Baldry & Glazebrook, 2003; Chabrier, 2003), recent results have started to show systemic variations (e.g. Bastian et al., 2010; Hopkins, 2018). At $z \sim 0$ local early type galaxies (ETGs) have shown evidence for the lower mass of the IMF slope to vary as a function of velocity dispersion (e.g. Cappellari et al., 2012; Conroy et al., 2013),

metallicity (e.g. Martín-Navarro et al., 2015b), and radial distance from the galactic center (e.g. Martín-Navarro et al., 2015a). However, mechanisms for such variations are still not well understood. Therefore, constraining the IMF in the early Universe is vital to determine how such variations may have been influenced by conditions prevalent in the Universe when the local ETGs were building up their stellar masses. Constraints on the early Universe IMF is also necessary to provide constraints to the cosmic SFH and to understand how the Universe transformed from hydrogen and helium to the current complex Universe.

The IMF of the $z \sim 3 - 5$ massive quiescent galaxies can be constrained using high-precision dynamical and stellar mass measurements. NIRSpec slit spectroscopy or NIRSpec IFU observations (see Section 4) can be used to constrain the dynamical masses of the galaxies. Given these early systems are compact and dense ($M_* \sim 10^{10} - 10^{11}$, $r_e \sim 0.5 - 2$ kpc (Straatman et al., 2014; Esdaile et al., 2020)), the baryonic matter is expected to dominate the kinematics, thus dynamical mass measurements are largely independent of the assumed dark matter halo profiles. This means that the dynamical mass is only contributed to by the stellar mass and thus the ratio of the dynamical mass to stellar mass (also known as the IMF mismatch parameter (e.g. Davis & McDermid, 2017)) can be used to understand the stellar populations via the IMF. JWST NIRSpec spectroscopy will also provide constraints to the rest-frame optical spectral shape of the $z \sim 3 - 5$ massive quiescent galaxies, which will provide strong constraints to stellar masses (Conroy, 2013). Therefore,

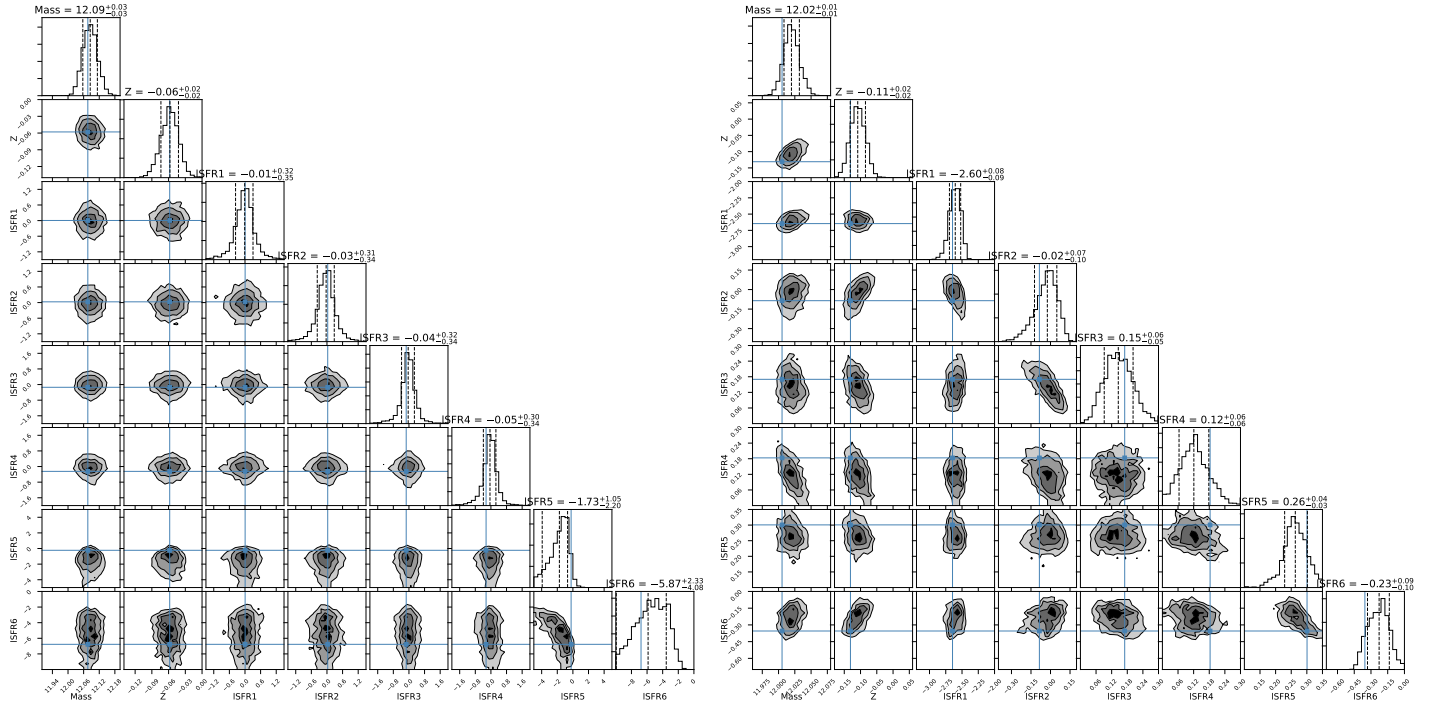


Figure 8. The one and two dimensional projections of the posterior probability distributions of the Markov Chain Monte Carlo simulations performed using PROSPECTOR. Out of the 15 free parameters only seven parameters; mass (in $\log_{10}(M_{\odot})$), metallicity (in $\log_{10}(Z_{\star}/Z_{\odot})$), and the 6 SFH bins (in $\log_{10}(M_{\odot}/\text{yr})$) are shown here for clarity. In **Left**: we show the corner plot of the single burst galaxy while in the **Right**: we show the corner plot of the galaxy with a complex SFH. In both scenarios, the posterior has been sampled well with no strong degeneracies between the parameters. In Figure 10 we show the recovery of the SFHs.

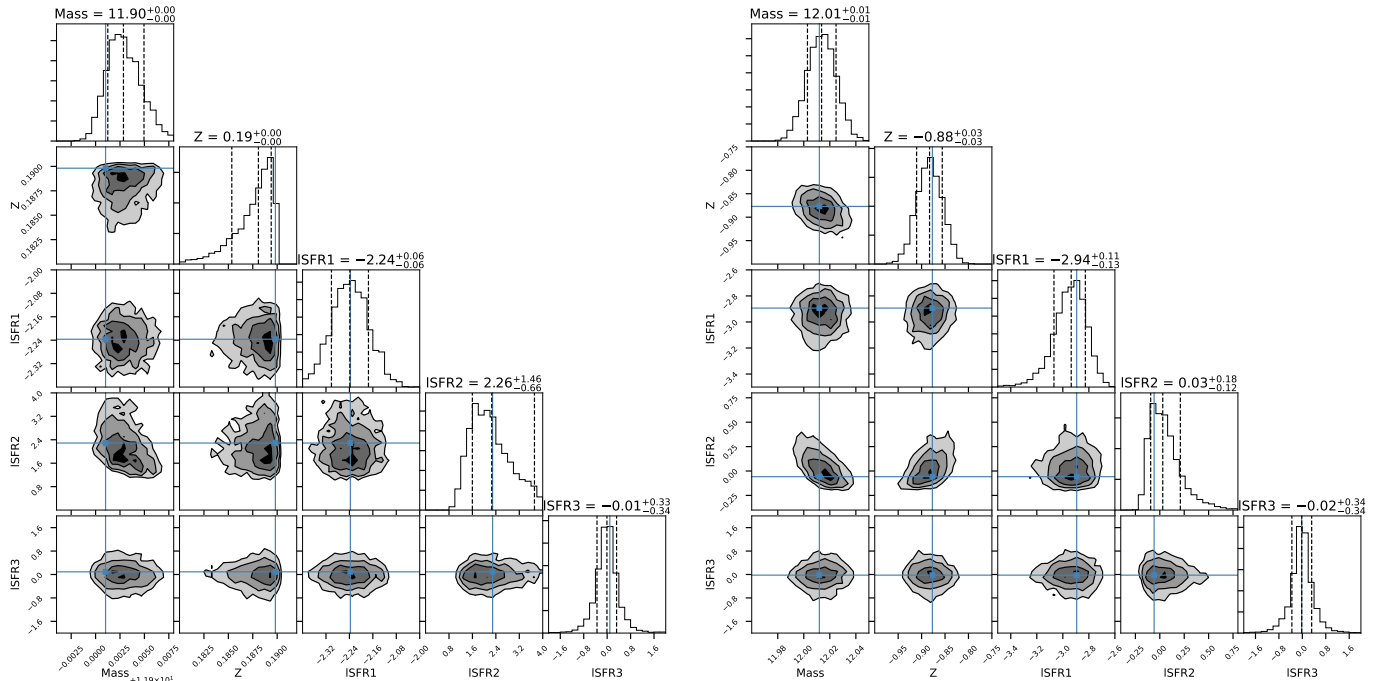


Figure 9. Same as Figure 8 but for 3 SFH bins. In Figure 10 we show the recovery of the two SFHs.

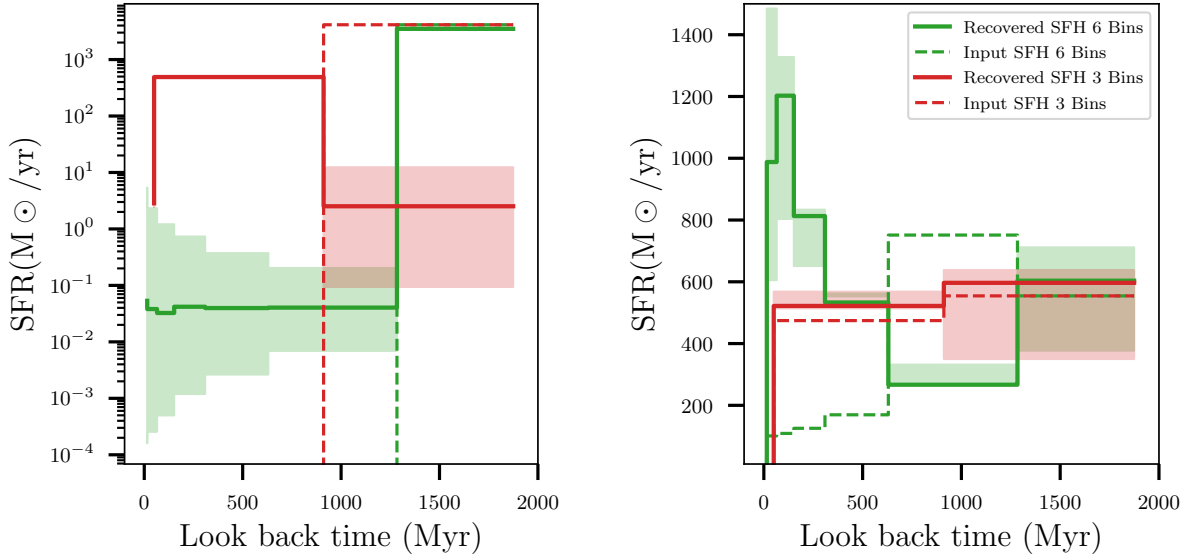


Figure 10. The recovery of SFHs based on full spectral + photometry fitting by the PROSPECTOR SED fitting code. Two observables are fit using PROSPECTOR, **Left:** one with short single star-burst and **Right:** an extended SFH. The 16th and 84th percentile are shown by the colour shading for each recovered SFH. The single burst SFH is well recovered with a SFH with 6 bins while the composite SFH is recovered well by a 3 bin SFH, thus some fine tuning of SFH bins are required to accurately recover the SFHs.

with JWST spectroscopy, stronger constraints on the IMF mismatch parameter can be obtained.

The IMF mismatch parameter can be compared with the distribution of the $z \sim 3 - 5$ galaxies in the stellar mass plane to see if there are differences in the inherent stellar populations of these galaxies perhaps indicating different formation scenarios. Given quiescent galaxies by definition do not have active star-formation, the ‘observed’ dynamical mass will only constrain the lower mass slope of the IMF. This is due to the lack of massive O, B type stars, which have relatively short life times of 10 – 100 Myrs compared to the long lived lower mass stars.

The IMF mismatch parameter is the only practical way to measure the IMF of unlensed individual massive quiescent galaxies at $z \sim 3 - 5$. As we showed in Figure 4, IMF sensitive spectral features such as the Na I doublet and the Wing–Ford band resulting from K and M dwarf stars require $S/N > 300$ to distinguish between different IMF slopes (van Dokkum & Conroy, 2010). Our NIRSpec simulations with ALF show that a $S/N \sim 350$ is required in the G395H/FL290LP grism/filter combination to recover the IMF slopes and reaching such levels even for the brightest $z \sim 3 - 5$ massive quiescent galaxies is not feasible due to the very high exposure times required.

Apart from the ‘observed’ IMF, the *relic* IMF of $z \sim 3 - 5$ massive quiescent galaxies can be reconstructed through spectrophotometric fitting of advanced SED fitting codes such as PROSPECTOR (private communication) and variable IMF chemical evolution codes such as galIMF (Yan et al., 2019). By providing IMF as an extra free parameter in SED fitting, the evolution of the IMF in the $z > 5$ Universe can

be constrained. However, time variation of the IMF, SFH, and α -element abundances are intricately connected (e.g. Martín-Navarro, 2016), therefore detailed stellar population modeling is required to understand degeneracies between them. $z > 5$ Universe is the time window when the $z \sim 3 - 5$ massive quiescent galaxies were forming the bulk of their stars. If these galaxies did indeed have top heavy IMFs in their star-formation phase (e.g. as formulated by Lacey et al. (2016), also see Gunawardhana et al. (2011); Nanayakkara et al. (2017, 2020)), this would lead to differences in the number of ionizing photons produced, the chemical enrichment and stellar wind and supernovae feedback processes. Such changes would be crucial to the re-ionization timescales of the Universe, thus, the reconstruction of the *relic* IMF in the $z > 6$ Universe is important to constrain the cosmological evolutionary models of the Universe.

4 DYNAMICAL PROPERTIES OF GALAXIES WITH JWST

The dynamical properties of massive $z \sim 3 - 5$ quiescent galaxies are an important quantity to constrain the evolutionary properties of massive galaxies in the early Universe. Through JWST slit or IFU spectroscopy, velocity dispersions, dynamical masses, stellar masses, sizes, and the evolution of the mass-size-velocity dispersion plane for quiescent galaxies at $z \sim 3 - 5$ can be constrained. Analyzing the $z \sim 3 - 5$ galaxies in this plane and comparing them with galaxies at lower redshifts is necessary to build up the cosmic evolutionary picture of quiescent galaxies and to determine how they evolve in the mass-size plane with cosmic time (e.g. Belli

et al., 2017a). Constraining kinematic properties is also important to determine whether these massive quiescent galaxies have undergone mergers in their evolutionary history (e.g. Belli et al., 2017b), which will shed further light into mass assembly and quenching processes in the early Universe.

4.1 Velocity dispersions through slit spectroscopy

JWST NIRSpec slit spectroscopy can be used to measure the velocity dispersions of $z \sim 3 - 5$ massive quiescent galaxies. In Figures 5 and 6 we show the recovery of the velocity dispersions of our mock NIRSpec S200A1 simulations. It is clear that with both grisms and filters, the velocity dispersion is converged to the input value of the mock simulations. In Section 3.1 we established that G235M/FL170LP grism/filter combination provides the best wavelength coverage and the necessary resolution to obtain the element abundances of $z \sim 3 - 5$ galaxies.

In terms of velocity dispersion, the G235M medium-resolution disperser of NIRSpec can obtain dispersions of $\sim 130\text{km/s}$ for a 2-pixel resolution element while the high resolution G235H disperser achieves a dispersion resolution of $\sim 50\text{km/s}$. Given the lowest velocity dispersion observed for $z > 3$ quiescent galaxies is $\sim 150\text{km/s}$ (Esdaile et al., 2020), the medium resolution grating is sufficient to obtain velocity dispersions of quiescent galaxies. We perform further mock JWST observations of a galaxy with $\sim 150\text{km/s}$ velocity dispersion and find that at a S/N of 30, the velocity dispersion can be recovered by the G235M/FL170LP grism/filter combination. Additionally, we find that the delivered S/N from G235M is higher than the S/N of G235H when binned to the same spectral resolution.

By obtaining a S/N of ~ 30 per pixel with JWST NIRSpec G235M/FL170LP observations, robust constraints can be obtained to the dynamical masses. For example, Esdaile et al. (2020) measured dynamical masses for four $z \sim 3 - 5$ massive quiescent galaxies with an accuracy of $\sim 20\%$. This was based on measurements of Balmer and Ca H & K absorption lines covering a total of $\sim 600\text{\AA}$ in rest-frame with a continuum S/N of $\sim 5 - 7$ achieved through spectral binning of 6\AA in the rest-frame. With NIRSpec, our simulations show that high quality spectra of such galaxies can be obtained with typical S/N of $\sim 30 - 40$ per pixel at similar resolution with a continuous coverage of $\sim 3000\text{\AA}$ in the rest-frame. They have no skyline contamination and reach an accuracy of $\sim 2 - 3\%$ for dynamical mass measurements. This higher level of accuracy will enable robust comparisons with mass-matched control samples of galaxies at $z \sim 2$, which can also be obtained as filler targets using the JWST NIRSpec multi-object spectroscopy (MOS) which utilizes the NIRSpec micro-shutter assembly (MSA).

4.2 Galaxy kinematics through IFU spectroscopy

JWST NIRSpec IFU spectroscopy can be used to obtain resolved kinematics of $z \sim 3 - 5$ massive quiescent galaxies.

Compared to ground based IFU spectroscopy, the JWST NIRSpec IFU provides many advantages for kinematics analysis. Higher spatial resolution can be obtained due to diffraction limited space-based observing at $2\mu\text{m}$ and is not limited by the lack of bright stars necessary for adaptive optics corrections to increase the seeing. Generally, non-AO observations are preferred for analysis of continuum sources with absorption line kinematics. This is because in kinematics the AO PSF imposes an interdependency between luminosity, velocity, and dispersion, thus more advanced deconvolution is necessary in each spectral plane of the original data cube (Davies & Kasper, 2012). This can be corrected for by robustly using emission line features (after accounting for beam smearing), however, for continuum features a PSF convolved step wise model for every pixel in the continuum and equivalent width would be required. This is hard to achieve even for bright sources (Thater et al., 2019). Additionally, the desired S/N is practically impossible to achieve even with the best ground based IFUs such as Keck/OSIRIS, where the majority of the absorption features for $z \sim 3$ galaxies exist in the H -band where the Strehl ratio is low ($\sim 10\%$). For example, for the two mock NIRSpec IFU simulations of two of the Esdaile et al. (2020) galaxies which we describe below, the total exposure time necessary to obtain resolved kinematics increases from $\sim 8 - 12$ hours with JWST/NIRSpec time to $> 40 - 100$ hours (based on the surface brightness of the galaxy) in ground based Keck/OSIRIS spectroscopy.

In order to investigate whether JWST NIRSpec IFU observations could recover the kinematics of $z \sim 3 - 5$ massive quiescent galaxies accurately, we perform full 2D mock IFU simulations to investigate the recovery of spatially resolved velocities with pPXF (Cappellari, 2017). We use empirical SSPs from Villaume et al. (2017) to generate mock 1.5 Gyr old galaxies with velocity dispersions consistent with the measurements in Esdaile et al. (2020). These model spectra are input into the JWST ETC, including their physical size and properties determined from modeling using *HST* H -band images. Several mock IFU cubes were then generated to obtain a suite of S/N values. Hernquist rotational models (Hernquist, 1990) were then applied to each simulated IFU observation, assuming a 45° inclination, with various rotational-to-velocity dispersion ratios (V_r/σ) to simulate galaxies with rotational support. A Hernquist model is chosen as suitable for modeling a rotating spheroidal star system; the estimated mass and the scale length (taken to be the effective radius of the galaxy), produce the velocity profile. The Plummer model (Plummer, 1911) produce similar rotational curves. Finally we used pPXF on the instrument calibrated data to fit for radial velocity and velocity dispersion.

In Figure 11 we show the recovery of both 3D-EGS-18996 and 3D-EGS-40032 2D kinematics. We note that the JWST ETC outputs $0.1''$ spaxels which do not account for drizzling, however, we expect in practice that drizzling will improve the sampling compared to what is shown here. Given the compact sizes and sharp decrease in S/N per spaxel, binning to this IFU spaxel scale is likely optimal for signal, while still

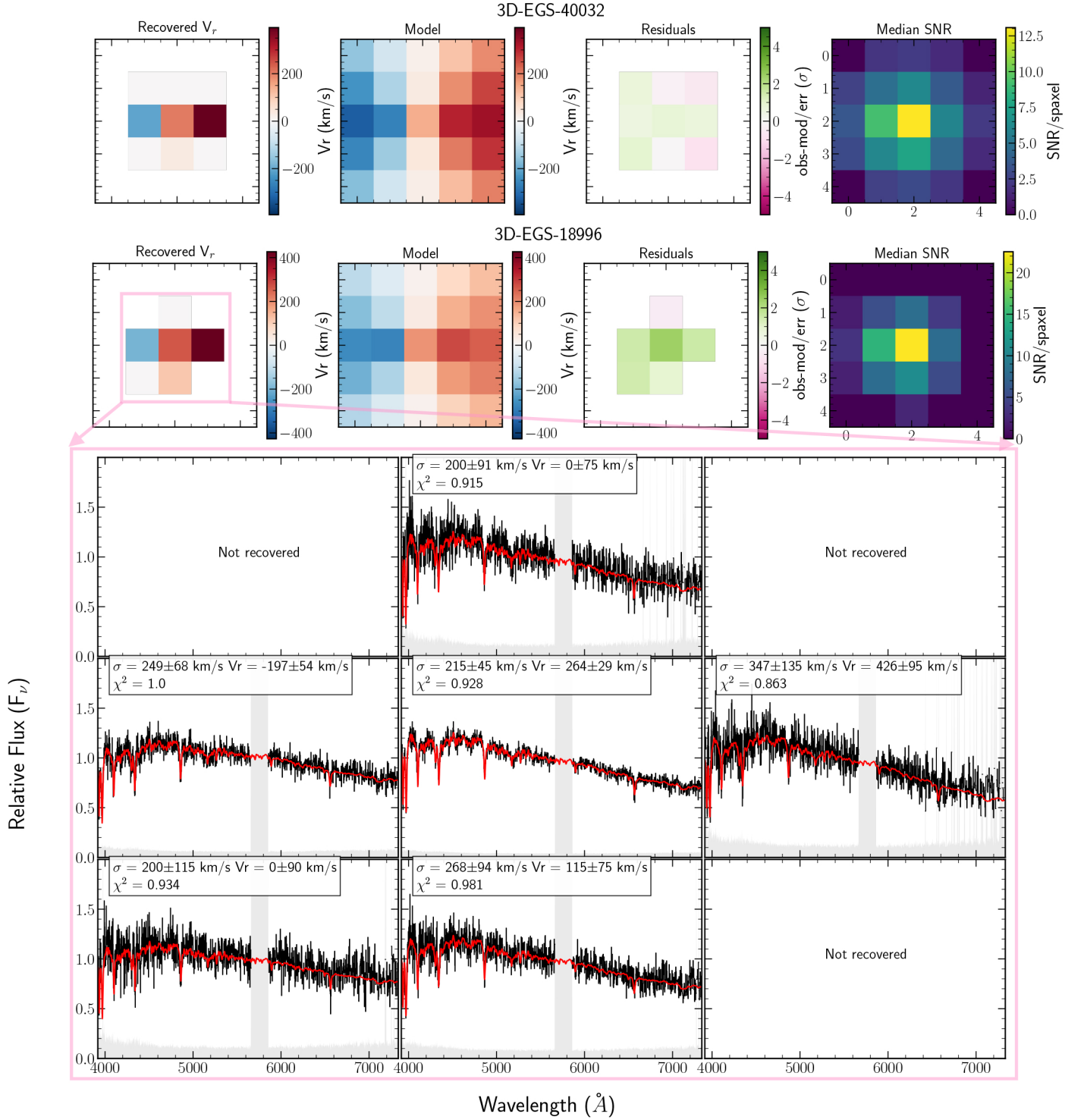


Figure 11. Simulated IFU observations for 2D kinematics recovery of two galaxies in the Esdaile et al. (2020) sample; 3D-EGS-40032 (G140M/F100LP grism/filter, 12h exposure) and 3D-EGS-18996 (G235H/F170LP grism/filter, 8h exposure). The chosen grism/filter combination optimizes the spectral ranges (which includes [OII] emission from 3D-EGS-40032), sensitivity, and resolving power to measure existing velocity dispersions for each galaxy. **Top: from left to right:** recovered 2D kinematics from simulated IFU cube (**left**) for a Hernquist 2D model of a rotationally supported galaxy and with an inclination of 45° (**middle-left**), the normalized residuals (**middle-right**) and median S/N/spaxel from the IFU cube. The simulation for 3D-EGS-40032 is in the top row with a $V_r/\sigma = 1.5$ and 3D-EGS-18996 is below with a $V_r/\sigma = 1.8$. **Bottom:** Recovered radial velocities and velocity dispersions for 3D-EGS-18996 per inner set of spaxels in the simulated IFU observations cube. Black lines are the simulated spectra, red lines are the best-fit and gray shaded area is the corresponding noise spectra. The spectral fit is only included for $0.85 < \chi^2 < 1.5$

allowing sufficient spatial scale to infer rotation. To assess the S/N requirements for the mock observations, this analysis was repeated for different exposure times. We found that a median S/N ~ 7 per spaxel is required in the adjacent to central pixels to recover a radial velocity and infer rotation with $> 2\sigma$ confidence. At this S/N V_r/σ can be constrained to $V_r/\sigma \sim 1.5$ in 3D-EGS-18996 and $V_r/\sigma \sim 1.3$ in 3D-EGS-40032 and confirm rotational support in these galaxies. Additionally, this would limit the underestimation in dynamical mass from 0.4 dex (for a $V_r/\sigma \sim 3$) to $\sim 0.1 - 0.15$ dex (from equation 5 Belli et al., 2017a) in both galaxies and allow for high precision IMF constraints without potential large systematic errors.

5 DISCUSSION AND CONCLUSIONS

In this analysis we have shown that the launch of JWST will address crucial observational challenges that currently limit our understanding of the abundance, formation, and evolutionary mechanisms of $z \sim 3 - 5$ quiescent galaxies. Given these galaxies provide insights into galaxy evolution in the $z > 6$ Universe, detailed analysis would determine how the first generation of galaxies in the Universe formed and evolved. Current cosmological models find it challenging to match the observed abundance of massive quiescent galaxies in the $z \sim 3 - 5$ Universe (e.g. Merlin et al., 2019), thus the analysis of the stellar populations and galaxy kinematics is vital to reconstruct the star formation and merger history of these galaxies.

The development of medium-band imaging instruments have allowed surveys like ZFOURGE Straatman et al. (2016) and FENIKS (Esdaile et al., submitted) to be carried out where the photometric redshifts can be obtained with high accuracy taking advantage of the increase spectral sampling of the split *H*, *J*, and *K* bands (e.g. Nanayakkara et al., 2016). JWST NIRSpec CLEAR spectroscopy provides the most prominent avenue to probe the completeness of these photometrically selected massive quiescent galaxies in the early Universe. This is driven by the multiplexing capability of NIRSpec along with the simultaneous continuous wavelength coverage between $0.6 - 5.3\mu\text{m}$. The large wavelength coverage is well suited to identify star-forming contaminants in $z \sim 3 - 5$ quiescent candidates. In Figure 3 we showed that the resolution and the sensitivity of NIRSpec CLEAR spectroscopy was sufficient to accurately distinguish between quiescent, post star-burst, and dusty star-forming galaxies. However, the spectral resolution of CLEAR spectroscopy is not sufficient to perform detailed analysis of element abundances to constrain the stellar population properties of $z \sim 3 - 5$ massive quiescent galaxies.

The optimal strategy to obtain spectral features to perform detailed analysis of stellar populations is to obtain deeper high-resolution JWST NIRSpec spectroscopy for samples that are already confirmed to be quiescent and are at redshift range of interest. Using simulated spectra from Villaume et al. (2017), we generated mock NIRSpec observations for

G235M/FL170LP, G235H/FL170LP, and G395H/FL290LP grism/filter combinations to identify the best combinations and the S/N required to recover accurate element abundances and velocity dispersions. We found that a S/N of ~ 30 is required to reach the necessary accuracy levels for element recoveries and that the G235M/FL170LP grism/filter combination is optimally suited to carry out the necessary observations. We found that the lower resolution of the G235M enables more efficient observations by achieving the necessary S/N level without compromising the accuracy, even when the higher resolution G235H grism is binned to the same velocity.

The G235M/FL170LP grism/filter combination is ideal to obtain coverage of rest-frame optical features of the $z \sim 3 - 5$ massive quiescent candidates. As an example we showed that Esdaile et al. (2020) sample will cover the crucial age, α -abundance, and metallicity sensitive indicators, all within $< 8\text{h}$ of exposure time. Compared to current best ground based spectroscopy, the improvement on S/N from JWST NIRSpec was found to be $7\times$ at similar velocity resolutions. As we showed in Figure 4, the Balmer absorption features are most sensitive to the ages, Mgb is strongly sensitive to the α abundance, and the overall metallicity is well constrained from the various Fe features that fall within the G235M/FL170LP wavelength coverage. With combined full spectrum fitting with softwares like *a1f*, the stellar population properties can be constrained to high accuracy.

In addition to the most recent star-formation episode that can be recovered from the Balmer absorption features, novel advanced SED fitting codes such as PROSPECTOR (Johnson et al., 2020) allow the full star-formation history of galaxies to be recovered. Using mock JWST G235M/FL170LP observations and photometry mapping the ZFOURGE COSMOS field coverage, we showed that spectrophotometric fitting can accurately recover the SFHs of galaxies to distinguish between different formation mechanisms, albeit with a dependence on the number of SFH bins. More work on understanding the role of the number and duration of SFH bins in accurately recovering the SFH of galaxies with short formation timescales is warranted.

Future advancements of SED fitting codes will allow IMF to be varied as an extra free parameter (i.e. PROSPECTOR, private communication). This will enable astronomers to perform robust statistical modeling of SFHs with variable IMFs in the early Universe. Recent studies have suggested that star-forming galaxies are likely to have higher fraction of high mass stars compared to the traditional Salpeter (1955) IMF (e.g. Gunawardhana et al., 2011; Nanayakkara et al., 2017) and recent semi-analytical models have started to implement such changes to their evolutionary models (Lacey et al., 2016). However, adding extra layers of free parameters could lead to larger degeneracies between the parameters. In Figure 8 we showed that within the context of 15 free parameters, PROSPECTOR posterior sampling does not show evidence for strong degeneracies but from Figure 10 it was evident that some fine tuning of the number of SFH bins are required for an accurate recovery of the SFH. Additionally, with the supe-

rior quality NIRSpec data, and advanced spectrophotometric fitting codes these extra degeneracies will be further constrained by the confident detections of multiple α -elements, Fe, and the suite of Balmer absorption lines. They will provide stringent constraints to metallicity, element abundances, and SFH timescales.

Apart from reconstruction of the SFHs, the integral field spectrographic capabilities of JWST/NIRSpec allows the kinematics of the $z \sim 3 - 5$ massive quiescent galaxies to be explored. In Figure 11 we showed through mock observations that the kinematics of galaxies similar to Esdaile et al. (2020) sample can be recovered. In addition to constraints to dynamical masses (and inferences about stellar population properties such as IMF), the kinematics of such galaxies provide vital clues to whether these massive galaxies already show ordered rotation or if they show the signatures of mergers. This can be used as an independent method to establish the formation pathways to early massive quiescent galaxies. Thus, future surveys with JWST will be able to determine whether the early massive quiescent galaxies could be formed within the first $\sim 1 - 2$ Gyr following Λ CDM hierarchical merger cosmology.

The advancements made in understanding the abundances, properties of the stellar populations, and formation scenarios of $z \sim 3 - 5$ massive quiescent galaxies through JWST, the next generation of cosmological simulations will be able to address the cosmic puzzle of how such galaxies in the early Universe were so efficient in building up stellar mass within short time-frames. This will allow additional constraints on galaxy evolution in the $z > 6$ Universe to be made, thus will provide more stringent constraints on reionization pathways and timescales of the Universe and the relative contribution of massive galaxies to the epoch of reionization.

ACKNOWLEDGMENTS

We thank Michael Maseda, Marijn Franx, and Joel Leja for helpful discussions. We also thank the staff at the James Webb Space Telescope Help Desk. T.N., K. G., M.D., and C.J. acknowledge support from Australian Research Council Laureate Fellowship FL180100060. This project made use of *astropy* (Astropy Collaboration et al., 2018), *matplotlib* (Hunter, 2007), and *pandas*.

REFERENCES

- Astropy Collaboration et al., 2018, *AJ*, 156, 123
- Baldry I. K., Glazebrook K., 2003, *ApJ*, 593, 258
- Bastian N., Covey K. R., Meyer M. R., 2010, *ARA&A*, 48, 339
- Bell E. F., de Jong R. S., 2001, *ApJ*, 550, 212
- Belli S., Newman A. B., Ellis R. S., 2017a, *ApJ*, 834, 18
- Belli S., et al., 2017b, *ApJ*, 841, L6
- Birkmann S. M., et al., 2011, in Heaney J. B., Kvamme E. T., eds, *Society of Photo-Optical Instrumentation Engineers (SPIE) Conference Series Vol. 8150*, Cryogenic Optical Systems and Instruments XIII. p. 81500B, doi:10.1117/12.893896
- Brinchmann J., Kunth D., Durret F., 2008, *A&A*, 485, 657
- Bruzual A. G., 2007, in Vazdekis A., Peletier R., eds, Vol. 241, *Stellar Populations as Building Blocks of Galaxies*. pp 125–132 (arXiv:astro-ph/0703052), doi:10.1017/S1743921307007624
- Cappellari M., 2017, *MNRAS*, 466, 798
- Cappellari M., et al., 2012, *Nature*, 484, 485
- Carnall A. C., et al., 2020, *MNRAS*, 496, 695
- Casali M., et al., 2007, *Astronomy and Astrophysics*, 467, 777
- Chabrier G., 2003, *Publications of the Astronomical Society of the Pacific*, 115, pp. 763
- Conroy C., 2013, *ARA&A*, 51, 393
- Conroy C., Gunn J. E., 2010, *ApJ*, 712, 833
- Conroy C., van Dokkum P., 2012, *ApJ*, 747, 69
- Conroy C., Dutton A. A., Graves G. J., Mendel J. T., van Dokkum P. G., 2013, *ApJ*, 776, L26
- Conroy C., Villaume A., van Dokkum P. G., Lind K., 2018, *ApJ*, 854, 139
- Davé R., Thompson R., Hopkins P. F., 2016, *MNRAS*, 462, 3265
- Davies R., Kasper M., 2012, *ARA&A*, 50, 305
- Davis T. A., McDermid R. M., 2017, *MNRAS*, 464, 453
- Esdaile J., et al., 2020, arXiv e-prints, p. arXiv:2010.09738
- Forrest B., et al., 2020a, *ApJ*, 890, L1
- Forrest B., et al., 2020b, *ApJ*, 903, 47
- Glazebrook K., et al., 2017, *Nature*, 544, 71
- Gunawardhana M. L. P., et al., 2011, *MNRAS*, 415, 1647
- Gunawardhana M. L. P., et al., 2020, *MNRAS*, 497, 3860
- Hernquist L., 1990, *ApJ*, 356, 359
- Hill A. R., van der Wel A., Franx M., Muzzin A., Skelton R. E., Momcheva I., van Dokkum P., Whitaker K. E., 2019, *ApJ*, 871, 76
- Hopkins A. M., 2018, *PASA*, 35, 39
- Hopkins P. F., et al., 2018, *MNRAS*, 480, 800
- Hunter J. D., 2007, *Computing In Science & Engineering*, 9, 90
- Johnson B. D., Leja J., Conroy C., Speagle J. S., 2020, arXiv e-prints, p. arXiv:2012.01426
- Kissler-Patig M., et al., 2008, *A&A*, 491, 941
- Kobayashi C., Nomoto K., 2009, *ApJ*, 707, 1466
- Kriek M., et al., 2016, *Nature*, 540, 248
- Kroupa P., 2001, *MNRAS*, 322, 231
- Kubo M., Tanaka M., Yabe K., Toft S., Stockmann M., Gómez-Guijarro C., 2018, *ApJ*, 867, 1
- La Barbera F., Ferreras I., Vazdekis A., de la Rosa I. G., de Carvalho R. R., Trevisan M., Falcón-Barroso J., Ricciardelli E., 2013, *MNRAS*, 433, 3017
- Lacey C. G., et al., 2016, *MNRAS*, 462, 3854
- Leja J., Johnson B. D., Conroy C., van Dokkum P. G., Byler N., 2017, *ApJ*, 837, 170

- Leja J., Carnall A. C., Johnson B. D., Conroy C., Speagle J. S., 2019, *ApJ*, 876, 3
- Madau P., Dickinson M., 2014, *ARA&A*, 52, 415
- Marchesini D., et al., 2010, *ApJ*, 725, 1277
- Marsan Z. C., Marchesini D., Brammer G. B., Geier S., Kado-Fong E., Labbé I., Muzzin A., Stefanon M., 2017, *ApJ*, 842, 21
- Martín-Navarro I., 2016, *MNRAS*, 456, L104
- Martín-Navarro I., Barbera F. L., Vazdekis A., Falcón-Barroso J., Ferreras I., 2015a, *MNRAS*, 447, 1033
- Martín-Navarro I., et al., 2015b, *ApJ*, 806, L31
- Merlin E., et al., 2019, *MNRAS*, 490, 3309
- Naidu R. P., Tacchella S., Mason C. A., Bose S., Oesch P. A., Conroy C., 2019, arXiv e-prints, p. arXiv:1907.13130
- Nanayakkara T., et al., 2016, *ApJ*, 828, 21
- Nanayakkara T., et al., 2017, *MNRAS*, 468, 3071
- Nanayakkara T., et al., 2020, *ApJ*, 889, 180
- Narayanan D., Davé R., 2012, *MNRAS*, 423, 3601
- Nomoto K., Tominaga N., Umeda H., Kobayashi C., Maeda K., 2006, *Nucl. Phys. A*, 777, 424
- Patel S. G., Hong Y. X., Quadri R. F., Holden B. P., Williams R. J., 2017, *ApJ*, 839, 127
- Pauldrach A. W. A., Hoffmann T. L., Lennon M., 2001, *A&A*, 375, 161
- Persson S. E., et al., 2013, *PASP*, 125, 654
- Plummer H. C., 1911, *MNRAS*, 71, 460
- Poggianti B. M., Barbaro G., 1997, *A&A*, 325, 1025
- Salpeter E. E., 1955, *ApJ*, 121, 161
- Saracco P., et al., 2020, *ApJ*, 905, 40
- Schreiber C., et al., 2018, *A&A*, 618, A85
- Segers M. C., Schaye J., Bower R. G., Crain R. A., Schaller M., Theuns T., 2016, *MNRAS*, 461, L102
- Sparre M., et al., 2015, *MNRAS*, 447, 3548
- Spitler L. R., et al., 2014, *ApJ*, 787, L36
- Steidel C. C., Strom A. L., Pettini M., Rudie G. C., Reddy N. A., Trainor R. F., 2016, *ApJ*, 826, 159
- Straatman C. M. S., et al., 2014, *ApJ*, 783, L14
- Straatman C. M. S., et al., 2016, *ApJ*, 830, 51
- Sutherland W., et al., 2015, *A&A*, 575, A25
- Tanaka M., et al., 2019, *ApJ*, 885, L34
- Thater S., Krajnović D., Cappellari M., Davis T. A., de Zeeuw P. T., McDermid R. M., Sarzi M., 2019, *A&A*, 625, A62
- Valentino F., et al., 2020, *ApJ*, 889, 93
- Vazdekis A., Sánchez-Blázquez P., Falcón-Barroso J., Cenarro A. J., Beasley M. A., Cardiel N., Gorgas J., Peletier R. F., 2010, *MNRAS*, 404, 1639
- Vazdekis A., et al., 2015, *MNRAS*, 449, 1177
- Villaume A., Conroy C., Johnson B., Rayner J., Mann A. W., van Dokkum P., 2017, *ApJS*, 230, 23
- Walcher J., Groves B., Budavári T., Dale D., 2011, *Ap&SS*, 331, 1
- Wellons S., et al., 2015, *MNRAS*, 449, 361
- Williams R. J., Quadri R. F., Franx M., van Dokkum P., Labbé I., 2009, *ApJ*, 691, 1879
- Yan Z., Jerabkova T., Kroupa P., Vazdekis A., 2019, *A&A*, 629, A93
- Yu H., Wang F. Y., 2016, *ApJ*, 820, 114
- de La Rosa I. G., La Barbera F., Ferreras I., de Carvalho R. R., 2011, *MNRAS*, 418, L74
- van Dokkum P. G., Conroy C., 2010, *Nature*, 468, 940